

Accepted Manuscript

Low velocity impact damage evaluation in fiber glass composite plates using pzt sensors

M.J. Santos, J.B. Santos, A.M. Amaro, M.A. Neto

PII: S1359-8368(13)00347-8

DOI: <http://dx.doi.org/10.1016/j.compositesb.2013.06.036>

Reference: JCOMB 2495

To appear in: *Composites: Part B*

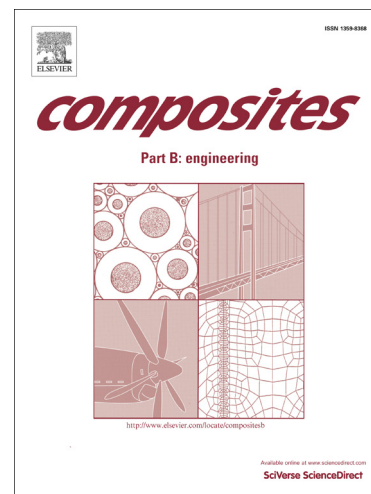
Received Date: 4 December 2012

Revised Date: 31 January 2013

Accepted Date: 14 June 2013

Please cite this article as: Santos, M.J., Santos, J.B., Amaro, A.M., Neto, M.A., Low velocity impact damage evaluation in fiber glass composite plates using pzt sensors, *Composites: Part B* (2013), doi: <http://dx.doi.org/10.1016/j.compositesb.2013.06.036>

This is a PDF file of an unedited manuscript that has been accepted for publication. As a service to our customers we are providing this early version of the manuscript. The manuscript will undergo copyediting, typesetting, and review of the resulting proof before it is published in its final form. Please note that during the production process errors may be discovered which could affect the content, and all legal disclaimers that apply to the journal pertain.



**LOW VELOCITY IMPACT DAMAGE EVALUATION IN FIBER GLASS COMPOSITE PLATES
USING PZT SENSORS**

M J Santos^{a,*}, J B Santos^a, A M Amaro^b, M A Neto^b

^aCEMUC, Department of Electrical and Computers Engineering, University of Coimbra, Polo II, Portugal

^bCEMUC, Department of Mechanical Engineering, University of Coimbra, Polo II, Portugal

*Corresponding author. Tel.: +351 239 796266; fax: +351 239 796247. E-mail: marioj@deec.uc.pt (M J Santos)

ABSTRACT

In this work PZT sensors are proposed to characterize the impact effects in fiber glass composite plates. To provide effective and reliable results the analysis was accomplished on samples submitted to multiple impacts, then guaranteeing the same testing conditions for different impact levels. The analysis of the impact effect has been made by two parameters; amplitude response and time shift. PZT sensors have been bonded to the samples in a pitch-and-catch configuration and the Lamb wave symmetrical mode (S_0) signal was used. The results demonstrate that the two evaluated parameters are able to characterise the different damage types occurring in these composites, as well as to evaluate their severity. It was also observed that amplitude predict well the defect size, whenever fiber-breakage occurs.

Keywords: A. Polymer-matrix Composites (PMCs); B. Defects; Impact behaviour; D. Ultrasonics.

1. Introduction

Fiber reinforced composite materials have been utilized for nearly four decades owing to their beneficial characteristics, such as stability, light weight and high stiffness. Particularly, in the automotive and aerospace industries the use of composites is justified by reducing structural weight with consequent fuel saving and improving performance [1]. During the service life, a composite structure is subjected to various loading conditions, which can give rise to various defects. The detection and quantification of

damage induced by low velocity impacts can be a difficult task because most damages are not visible on the external surface. In fact, the impact energy is absorbed through remarkable internal damage mechanisms without exterior signs detectable by visual inspection. Various types of damages, like delaminations, fiber-breakage, matrix cracking and fiber-matrix interfacial debonding can occur, leading to structural failure. The impact damage is considered as the primary cause of in service damage composites and can reduce the compressive residual strength up to 60%. [2-5]. The flexural strength can also be significantly reduced [6]. Delaminations are prone to occur at interfaces between different oriented layers due to mismatch bending that lead to development of interlaminar shear stresses at those interfaces [7]. Under tensile loading the existence of the delamination promotes a drop of strength [8-11], but its size does not influence significantly the value of tensile strength [11]. The poor tolerance to accidental low velocity impacts of the composite laminates is yet a limitation to their use in many applications in some industries [12]. The reduced compressive strength due to impact is believed to be the result of multiple delaminations presence. Suemasu et al [13] concluded that the load carrying capability of the delaminated plate is reduced by the delamination propagation, and the strength of the damaged plate is strongly dominated by the beginning of the delamination growth. On the other hand, during the manufacturing process, routine maintenance operations or in-service conditions, some components can be subjected to repeated impacts at localized positions [14,15]. Sevkat et al [15] studied the effect of repeated impacts on the response of composites and concluded that the lay-up sequence has significant effect on the repeated impact response of the hybrid composites, and that repeated impacts can caused very quick damage accumulation and promotes a progression of the damage. When the load reaches a critical level, the crack will extend and the failure occurs.

Recently, damage detection through ultrasonic guided waves, such as Lamb waves, has been gained increasing importance due to the possibility of inspecting large composite structures. Once excited, the Lamb waves can propagate all over considerable distances. Thus, a receiver positioned on the structure at a remote position can collect the propagation signals over the path between transmitter and receiver, providing information about eventual surface defects or internal cracks. Several studies using Lamb waves for damage detection in composite materials have been reported in literature. Valdes et al [16] used the Lamb wave time of flight to locate a delamination in a composite beam. Zang et al [17] employed also time domain analysis and artificial neural networks (ANN) to detect structural damages. Short-time Fourier

transform (STFT) were used by Kim et al [18] for damage detection in rolling bearings. With the aid of Wavelet transform, Lemistre et al [19] and Su et al [20] located delamination in carbon fiber composite plates. Paget et al [21] developed a new wavelet transform for energy impact prediction in a composite panel.

The generation of Lamb waves by conventional transducers has some limitations because they are relatively large and expensive. An emerging technique based on piezoelectric lead zirconate titanate (PZT) sensors has the potential to improve significantly the structural health monitoring (SHM). These sensors are small, lightweight, inexpensive, and can be produced in different geometries. They can be bonded on the structures surface, mounted inside built-in structures and can even be embedded between the structural and non-structural layers of a complete construction [22]. Banks et al. [23] were probably the first ones to evaluate damages with PZT sensors. Since then, several authors have studied the applicability of these sensors in different fields, namely in damage detection [24], defects location using distributed sensors [25,26] and wavelet signal processing [26], delamination evaluation based in the ratio of the power spectrum densities for different propagation modes [27] and by analysing modal frequencies [28] or detection of transverse crack and delamination in cross-ply laminates [29]. More recently, localization and monitoring of damages in honeycomb structures using PZT arrays [30], instantaneous delamination detection by comparing time delays of A_0 mode [31] and diagnosis of damage using in a modified time reversal method [32], are examples of potential practical applications of the PZT sensors.

This work aims to evaluate the severity of defects caused by multiple impacts in fiber glass composites by measuring some parameters, like signal amplitude and propagation time shift. The main contribution of this paper deals with the use of guided waves (Lamb waves) to characterize the effects of multiple impacts in laminate composites that to the best of our knowledge, there have no previous attempts.

2. Theory

Many authors have considered the use of Lamb waves for non-destructive testing. Rose [33], summarized the potential of these waves for damage detection and characterization in terms of the possibility of inspection an entire cross sectional area with a single direction displacement, inspection of large insulated or coated structures, no requiring complex motion devices, good sensitivity, low energy consumption and low cost. However, the use of those guided waves can be troublesome due to the propagation of multiple

modes, the dispersive character of the modes, and also the waves reflected in boundaries that can mask the signal of interest. Normally, the fundamental symmetric (S_0) and anti-symmetric (A_0) modes are selected to be used in practice due to their better time discrimination when compared with higher order modes.

PZT ceramics provide excellent performance in Lamb wave generation and acquisition. They are called active sensors due to its dual sensing and excitation characteristics. Typically, working in the kHz range, it is possible to obtain a few hundreds of mV in sensing, using a tone burst excitation signal of 10 V.

The strain $\varepsilon(x)$ induced by a plate-mounted PZT perfectly bonded to the structural surface has a response given by [22]

$$\varepsilon(x) = i\varepsilon_a (\sin(kL/2)) e^{i(kx - \omega t)} \quad (1)$$

where ε_a is the induced strain over the PZT length L and k is the wavenumber of the propagation mode in the plate. The response follows a sinusoidal variation with respect to the parameter $kL/2$ and the response peaks are observed at odd multiples of $\pi/2$.

The optimal excitation frequencies can be obtained by

$$f = \frac{v}{L} \left(n + \frac{1}{2} \right) \quad (n = 0, 1, 2, \dots) \quad (2)$$

where v is the Lamb wave velocity of the propagating mode in the material. The thickness selection has to take into account the maximum voltage allowed by the PZT without depolarising, that is around 250-300 V/mm [34].

Velocity measurements and consequent identification of ultrasound bulk waves are usually possible using the time of flight method. Considering the time difference between n^{th} peaks of the signal for two different locations, the propagation velocity can be easily calculated, if the shape of the signal remains the same. In the presence of dispersive waves like Lamb waves, frequency domain techniques are demanded for correct velocity evaluation and respective mode identification. Using the phase spectrum method [35] the phase velocity is given by

$$v_p = \frac{2\pi f D}{\Delta\varphi} \quad (3)$$

where $\Delta\varphi$ is the difference in the phase spectrum of two signals collected for a distance between them of D and f is the frequency.

3. Materials and experimental procedure

3.1 Composite laminates and mechanical properties

The laminates are composed of glass fiber Prepreg TEXIPREG® ET443 (EE190 ET443 Glass Fabric PREPREG from SEAL, Legnano, Italy) and have been processed in agreement with the manufacturer recommendations, using the autoclave/vacuum-bag moulding process. That processing consists of several steps: make the hermetic bag and apply 0.05 MPa vacuum; heat up to 125°C at a 3–5°C/min rate; apply a pressure of 0.5 MPa when the temperature of 120–125°C is reached. Then, the pressure and temperature are maintaining for 60 min, and finally cool down to room temperature maintaining the pressure. The laminates were fabricated on the four stacking sequences referred in Table 1, having a useful square shape of $300 \times 300 \times t$ [mm] (where t is the thickness). Three specimens of each stacking type have been used for testing. The mechanical properties of the glass/epoxy unidirectional composite laminates were obtained according the standards ASTM D3039; ASTM D3518 and ASTM D4255, and are presented in Table 2. Five specimens with 16 unidirectional plies $[0]_{16}$ were analyzed, making use of an electromechanical tensile testing machine (INSTRON 4206) of 50 kN load capacity. The tensile load was applied under stroke control with strain rates of 1.5 mm/min and 2 mm/min for the shear modulus and the other parameters, respectively.

3.2 Lamb waves in composite laminates

For detection and identification of the Lamb waves in the laminates the setup shown in Fig.1 has been used. Two Panametrics transducers with central frequency of 500 kHz were coupled to the laminate plates by plexiglas blocks with variable inclination. The transducers were glued to the blocks and coupling gel was utilized between blocks and the laminate plates. A Panametrics pulser/receiver generated the signals and a digital oscilloscope was used to visualize them after propagation on the plate. Then, the signals were transferred via a USB port to the computer for processing.

The symmetrical S_0 mode was selected, because the excitation of A_0 mode is not possible according to the co-incidence principle [36]. A typical collected signal is presented in Fig. 2.

The correct inclination for the blocks was obtained maximizing the amplitude of the collected signals. For the selected A sample the inclination was around 40°, which is according to the co-incident principle. The phase velocity presented in Fig. 3, was obtained using the phase spectrum method for two signals collected

5 cm apart in 0° direction. The considered frequency range for the spectrum was 200 to 500 kHz due to the downshift frequency related to the filtering effect of the laminate composites. The small decreasing behaviour of the phase velocity is expected according to the theory in the low frequency regime.

Using the previous set-up described in Fig.1 and proceeding with a rotation increment of 10° between each measurement, the wave propagation directivity patterns for S_0 mode were obtained for all analysed samples. For comparison purposes, an additional unidirectional fiber sample was tested, having a $[0]_{16}$ stacking sequence and 2.1 mm in thickness. Fig.4 illustrates the results for samples A and the $[0]_{16}$ one. As expected, for the unidirectional sample, the velocity for 0° direction is higher than the corresponding one for 90° direction, while for samples A the velocity is roughly the same in the cross directions. The results for the B, C and D samples were found to be similar to samples A.

3.3 Guided wave propagation with PZTs

For Lamb waves generation the used PZT sensors were cut in square pieces of $7\bar{7}$ mm from a PZ29 bar of 0.4 mm in thickness. For excitation, an arbitrary waveform generator (Tektronix AFG3022) was used to produce a 3-cycle toneburst with a Hanning window that was previous synthesized in Matlab. This windowing technique is used to narrow the signal bandwidth and to concentrate the maximum amount of energy into the desired frequency with a minimum spreading to neighbor frequencies. The signal was 10 V in amplitude. The PZT sensors were mounted in a pitch and catch configuration and the signals were collected as mentioned in section 3.2. The complete setup using a 1 mm thickness aluminium plate is presented in Fig. 5.

Fig. 6 shows the behaviour of the experimental normalized voltage amplitude at the receiver for a frequency sweeping from 100 kHz to 500 kHz as well as the theoretical values obtained from equation (1). The difference between the traces is related specifically to the imperfect coupling between the PZT and the plate, and also to the small discrepancies in PZT length. Nevertheless, if optimal resonance frequency is desired, which is mostly the case; the method could be used with reasonable accuracy. Similar results are reported by Giurgiutiu [22] that mentions the necessity of an effective PZT length adjustment to about 90% of its real length.

For the considered aluminium plate, the A_0 mode has the predicted response shown in Fig.7. Experimentally, it was not possible detecting this mode, as expected. The reason for that is probably related to the coupling medium used between the PZT and the plate.

For the composite plate, the PZT sensors were mounted 100 mm apart on the surface using conductive glue. A frequency sweep allowed verifying that the maximum signal in the receiver was obtained at 320 kHz. Using time of flight, it has easily been proved that the signal corresponded to the fundamental symmetrical mode S_0 . A typical signal propagating in a composite plate is presented in Fig. 8, showing the direct signal and the reflection from the plate edge.

4. Results and discussion

4.1 Impact tests analysis

Low velocity impact tests were produced using a drop-weight testing machine Instron-Ceast 9340 with a hemispherical impactor of 10 mm in diameter and a mass of 3.4 kg. The specimens were centrally supported. Fig. 9 represents the typical energy versus time curves obtained for samples A. The beginning of the curve plateau energy coincides with the loss of contact between the striker and the specimen, and this energy level corresponds to the absorbed one by the specimen [37]. In this context the dissipated energy is calculated as the difference between the absorbed energy and the energy at the peak load.

As the used glass plates are translucent the damage images were obtained by photography collected from the opposite side of the impact (back face). Images for the A, B, C and D samples showing the damages after suffering the last impact are shown in Fig. 10. The different damage shapes and sizes are essentially due to the stacking sequences, thicknesses and used energies. Fig. 10 (a) and (b) show a damage, which shape presents two lobes oriented on the fibers direction of the adjacent lower ply (0°), while samples in (c) and (d) do not reveal those two lobed shape because of the presence of multiple superposed delaminations at the several interfaces among the different oriented layers.

According to Sevkát et al [15], when the energy absorbed by the composite is small, the impactor bounced back and the damage area is also small. If a major energy of impactor is absorbed by the composite various modes of damage can appear with the consequent increase in size. Such is demonstrated by the graphical results outlined in Fig. 11 and 12. Fig. 11 shows the typical energy-time and load-time curves for the 15th impact carried out with energy of 1 J for samples A, B and C. It can be observed the higher load is obtained for the specimen C corresponding to the lower absorbed energy. On the other hand, the specimen A shows a higher absorbed energy and a lower load. The curves for the other impact numbers are similar. In Fig. 12 is presented the relation between the damage area and the number of impacts for all tested samples. For all kind of samples it is observed a damage area increasing with the number of impacts. However, that

increasing is more pronounced for the samples A than for samples B and C, considering the same impact energy (1 J), due to the lower thickness presented by the A ones. Also, samples B, C and D were submitted to higher energies, ranging from 3 to 10 J, leading to a jump in the damage area. The observed damage area variations, for all tested samples, agree with the higher absorbed energy with the impacts number according to the results shown in Fig. 9 and 11.

In order to observe changes in the morphological composition of the composites after impacts, namely fibers-breakage, a metallographic analysis was performed using optical microscopy in Zeiss HD100 equipment. The results showed that fibers-breakage appear after the 1st impact for samples A, 21st impact for samples B, 3rd for samples C, and 14th impact for samples D.

4.2 Pitch and catch evaluation of the multiple impacts

For evaluation of the impact effects in the fiber composite plates it was used the methodology presented in section 3.3. A pair of PZT sensors was previously bonded on each plate and after each impact the signals were acquire and processed. Next, the damage area was correlated with ultrasound parameters, like the amplitude and time shift as they provided the best results. The normalized peak to peak amplitude versus damage area for samples A is illustrated in Fig. 13. A high linear correlation between these two parameters ($R^2=0.968$) was obtained. Concerning to samples C, a high correlation was also observed. Unlike, samples B and D presented very low correlation values. As samples A and C present broken fibers from the beginning of the tests and samples B and D only for the last impacts, it can be inferred that the broken fibers influence greatly the amplitude parameter.

The time shift parameter was measured correlating the received signal with a benchmark signal (obtained from a reference plate without damage). For this purpose, a cross-correlation processing technique was used in order to improve the time resolution and also due to the slightly dispersive behaviour of the S_0 Lamb wave mode. This technique, widely used in signal processing [38,39], measures the similarity between two waveforms as a function of the time-lag applied to one of them. The discrete cross-correlation function between two signals $y_1(i)$ and $y_2(i)$ is given by

$$R(s) = \frac{\sum_{i=1}^N y_1(i) y_2(i+s)}{\sqrt{\sum_{i=1}^N y_1(i)^2 \sum_{i=1}^N y_2(i+s)^2}} \quad (4)$$

where s is the time shift between signals and N is the number of samples. The time shift s is obtained for the maximization of the function $R(s)$. Fig. 14 depicts the time shift between the reference signal and the signal after the 19th impact carried out on a selected A sample. The damage area versus time shift is shown in Fig. 15. It is observed an increase of the time shift with the damage severity, which is a consequence of a plate deformation that changes the ultrasound wave propagation path. The time shift approach was also applied to the other ones. For samples A, C and D a high linear correlation between the time shift and defect size was observed. For samples B, that correlation is lower. The results for amplitude and time shift parameters are summarized in Table 3.

Concerning the fibers-breakage, the amplitude appears as a useful parameter to predict its occurrence. In fact, for the samples A and C where the fibers-breakage was observed after the 1st a 3rd impacts, respectively, the correlations between the damage area and amplitude are high. On the contrary, for samples B and D where the fibers-breakage happened only for a higher impacts number, the correlations are low.

Considering the results for the time shift (see table 3), good correlation is always possible for damage size (moderated for samples B) independent of fibers-breakage occurrence.

5. Conclusions

The presented work demonstrates the suitability of PZT sensors for impact defects evaluation in fiber glass composite plates.

Experiments using conventional ultrasonic transducers with variable inclination, together with phase spectrum method allowed identifying S_0 Lamb wave mode in low frequency regime. The obtained directivity patterns are according to expectations. An appropriate setup was used for S_0 mode tuning of PZT sensors bonded in aluminium and fiber glass plates giving results according to the theory. Different types of samples fabricated with different stacking sequences were impacted using a pressure-assisted drop-weight testing machine. It was observed that the absorbed energy increases with the number of impacts with the consequent increase in the damage area. The stacking sequence influences the damage area due to the increased number of interfaces between layers with different orientations, which can promote the appearing and propagation of damages.

Multiple impacts were performed in each fiber glass composite samples to guarantee the same test conditions for different impact levels. After each impact, amplitude and time shift were measured. A high accuracy technique based on cross-correlation function was used to the time shift evaluation. Amplitude measuring shows high linear correlation with defect size only when fiber-breakage exists. On the other hand, time shift seems to be a better parameter for defect size estimation. This work proved that the amplitude and time shift parameters can usefully be used to estimate the damage areas and to predict the existence of fibers-breakage in laminates. Future work will be developed using others stacking sequence and different composite materials as the CFRP in order to evaluate the practicability of the used parameters for damage characterization.

References

1. Shimokawa T, Hamaguchi Y. Distributions of Fatigue Life and Fatigue Strength in Notched Specimens of a Carbon Eight-Harness-Satin Laminate. *J Compos Mater* 1983;17: 64-76.
2. Amaro AM, Reis PNB, Moura MFSF, Santos JB. Damage Detection on Laminated Composite Materials Using Several NDT Techniques. *Insight* 2012;54:14-20.
3. Abrate S. Impact on Laminated Composite Materials. *Appl Mech Rev* 1991;44:155-191.
4. Cantwell WJ, Morton J. Comparison of the low and high velocity impact response of CFRP. *Composites* 1989;20:545-551.
5. de Moura MF, Marques AT. Prediction of low velocity impact damage in carbon-epoxy laminates. *Compos Part A: Appl S* 2002;33:361-368.
6. Amaro AM, de Moura MF, Reis PB. Residual Strength after Low Velocity Impact in Carbon-Epoxy Laminates *Mater Sci Forum* 2006;624:514-516.
7. Moura MFSF, Gonçalves JPM. Modelling the Interaction between Matrix Cracking and Delamination in Carbon-epoxy Laminates under Low Velocity Impact. *Compos Sci Technol* 2004; 64: 1021-1027.
8. Reis PNB, Ferreira JAM, Antunes FV, Richardson MOW. Effect of Interlayer Delamination on Mechanical Behavior of Carbon/Epoxy Laminates. *J Compos Mater* 2009; 43: 2609-2621.
9. Mittelman A, Roman I. Tensile Properties of Real Unidirectional Kevlar/Epoxy Composites. *Composites* 1990; 21: 63-69.

10. Ryder JT, Crossman FM. A Study of Stiffness, Residual Strength and Fatigue Life Relationships for Composite Laminates. NASA CR-172211, 1983.
11. O'Brien TK, Rigamonti M, Zanotti C. Tension Fatigue Analysis and Life Prediction for Composite Laminates. *Int J Fatigue* 1989; 11: 379-393.
12. Collombet F, Bonini J, Lataillade JL. A Three-dimensional modelling of low velocity impact damage in composite laminates. *Int. J Numer Meth Eng* 1996; 39:1491-1516.
13. Suemasu H, Sasaki W, Ishikawa T, Aoki Y. A numerical study on compressive behavior of composite plates with multiple circular delaminations considering delamination propagation. *Compos Science and Technology* 2008;68(12):2562-2567.
14. Icten BM. Repeated impact behavior of glass/epoxy laminates. *Polym Compos* 2009;30:1562-1569.
15. Sevkat E, Liaw B, Delale F, Raju B. Effect of Repeated Impacts on the Response of Plain-Woven Hybrid Composites. *Compos Part B: Eng* 2010;41:403-413.
16. Valdes SH, Soutis C. A structural health monitoring system for laminated composites. In: *Proceedings of DETC*. Pittsburgh, PA, USA, 2001. p. 2013–2021.
17. Zang C, Friswell MI, Imregun, M. Structural damage detection using independent component analysis. *Structural Health Monitoring: An International Journal* 2004; 3(1):69–83.
18. Kim YY, Kim EH. Effectiveness of the continuous wavelet transform in the analysis of some dispersive elastic waves, *J Acoust Soc Am* 2001;110(1):1–9.
19. Lemistre M, Balageas DL. Structural health monitoring system based on diffracted Lamb wave analysis by multiresolution processing. *Smart Mater Struct* 2001;10:504–511.
20. Su Z, Ye L, Bu X. A damage identification technique for CF/EP composite laminates using distributed piezoelectric transducers. *Compos Struct* 2002;57:465–471.
21. Paget CA, Grondel S, Levin K, Delebarre C, Damage assessment in composites by Lamb waves and wavelet coefficients, *Smart Mater Struct* 2003;12:393–402.
22. Giurgiutiu V. *Structural Health Monitoring with Piezoelectric Wafer Active Sensors*. Academic Press, 2008.
23. Banks HT, Smith RC, Wang Y. *Smart material structures: Modeling, estimation and control*. Masson, Paris: John Wiley & Sons, 1996.

24. Kessler SS, Spearing SM, Soutis C. Damage detection in composite materials using Lamb wave methods. *Smart Mater Struct* 2002; 11: 269–278.
25. Diamanti K, Hodgkinson, JM, Soutis C. Detection of low-velocity impact damage in composite plates using Lamb waves. *Struct Health Monit* 2004; 3: 33-41.
26. Su Z, Ye L, Bu X., A damage identification technique for CF/EP composite laminates using distributed piezoelectric transducers. *Compos Struct* 2002;57:465–471.
27. Kim YH, Kim DH, Han JH, Kim CG. Damage assessment in layered composites using spectral analysis and Lamb wave. *Compos: Part B* 2007;38:800–809.
28. Valdes SHD, Soutis C. Delamination detection in composite laminates from variations of their modal characteristics. *J. Sound Vib.* 1999;228:1-9.
29. Toyama N, Noda J, Okabe T. Quantitative damage detection in cross-ply laminates using Lamb wave method. *Compos Sci Tech* 2003;63:1473–1479.
30. Chakraborty N, Rathod VT, Mahapatra DR, Gopalakrishnan S. Guided wave based detection of damage in honeycomb core sandwich structures. *NDT Int* 2012;49:27-33.
31. Yeum CM, Sohn H, Ihn JB, Lim HJ. Instantaneous delamination detection in a composite plate using a dual piezoelectric transducer network. *Compos Struct* 2012; 94:3490-3499.
32. Watkins R, Jha R. A modified time reversal method for Lamb wave based diagnostics of composite structures. *Mech Syst Signal Pr* 2012;3:345-354.
33. Rose JL. A vision of ultrasonic guided wave inspection potential. In: *Proceedings of the Seventh ASME NDE Topical Conference NDE-Vol. 20* 2001. p. 1–5.
34. Su Z, Ye L, Su YL. Guided Lamb waves for identification of damage in composite structures: A review. *J Sound Vib* 2006; 295:753-780.
35. Sachse W, Pao YH. On determination of phase and group velocity of dispersive waves in solids. *J Acoust Soc Am* 1978;49(8):4320-4327.
36. Santos M, Ferreira A, Perdigão J. Practical considerations on ultrasonic guided wave propagation: immersion and contact methods. *Mater Eval* 2004;62(4):443-449.
37. Río TG, Zaer R, Barbero E, Navarro C. Damage in CFRPs due to low velocity impact at low temperature. *Compos Part B-Eng* 2005; 36: 41-50.

38. Foster SG, Embree PM, O'Brien WD. Flow Velocity Profile via Time-Domain Correlation: Error Analysis and Computer Simulation. IEEE Trans Ultrason Ferroelect Freq Contr 1990;37(3):164-175.
39. Hein IA, O'Brien WD, A Real-Time Ultrasound Time-Domain Correlation Blood Flowmeter: Part II. IEEE Trans Ultrason Ferroelect Freq Contr 1990;40(6):776-785.

ACCEPTED MANUSCRIPT

Figures caption

Fig. 1. Experimental setup for Lamb wave detection and identification.

Fig. 2. Typical collected signal for the laminate composite plate.

Fig.3. Experimental S_0 phase velocity for samples A.

Fig. 4. S_0 wave propagation directivity patterns for samples: (a) $[0]_{16}$; (b) A.

Fig. 5. Experimental setup using an aluminium plate.

Fig. 6. Normalized S_0 Lamb wave tuning for a 7 mm length PZT placed on 1 mm thickness aluminium plate.

Fig. 7. Normalized A_0 Lamb wave tuning for a 7 mm length PZT placed on 1 mm thickness aluminium plate.

Fig. 8. Fundamental symmetrical S_0 mode in the composite plate.

Fig. 9. Typical energy versus time curves for samples A.

Fig. 10. Damages occurred after the last impact for samples: (a) A (19th); (b) B (22nd); (c) C (27th); (d) D (19th).

Fig. 11. Typical load-time and energy-time curves for laminates impacted at 1 J, after the 15th impact.

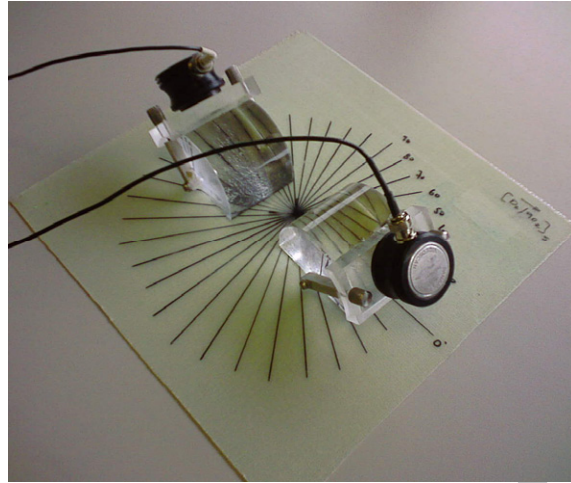
Fig. 12. Damage area versus number of impacts for all studied samples.

Fig. 13. Signal amplitude versus damage area for samples A.

Fig. 14. Signals for a reference selected sample A and after 19th impact.

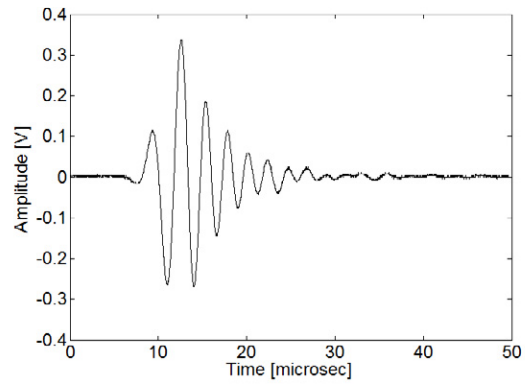
Fig. 15. Time shift versus damage area for samples A

Fig. 1



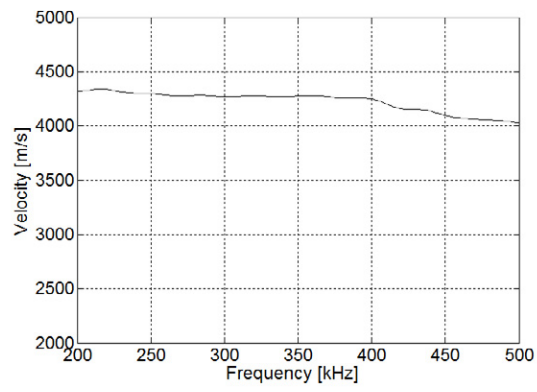
ACCEPTED MANUSCRIPT

Fig. 2



ACCEPTED MANUSCRIPT

Fig. 3



ACCEPTED MANUSCRIPT

Fig. 4

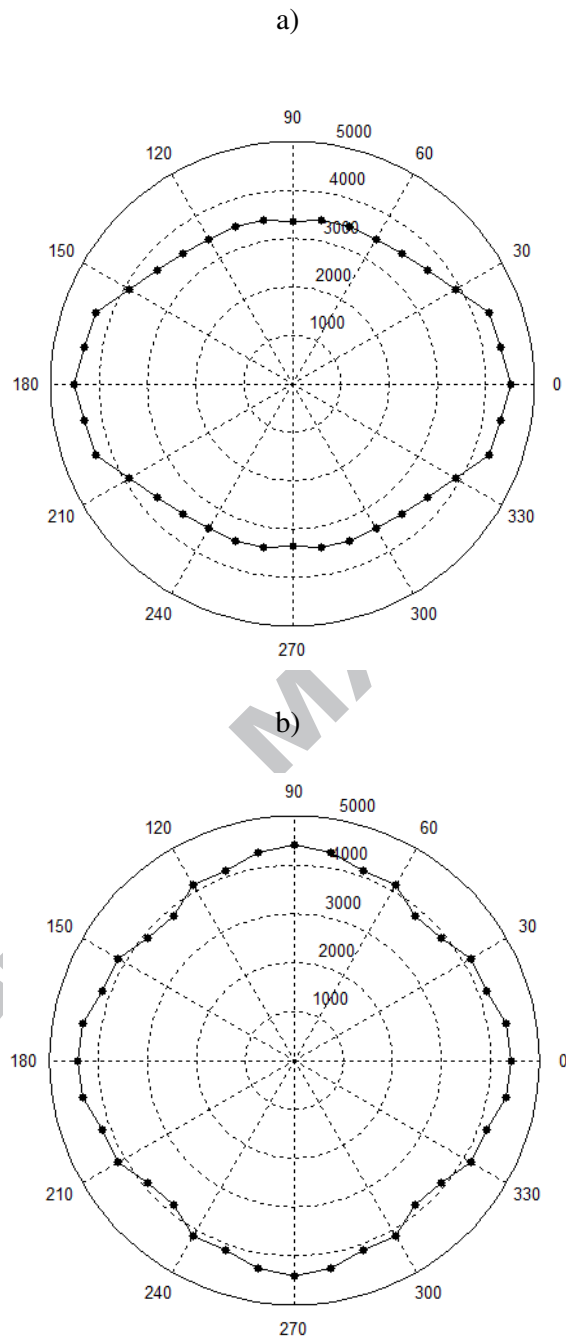
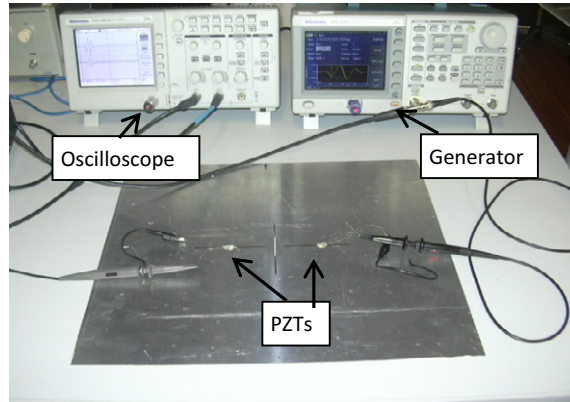
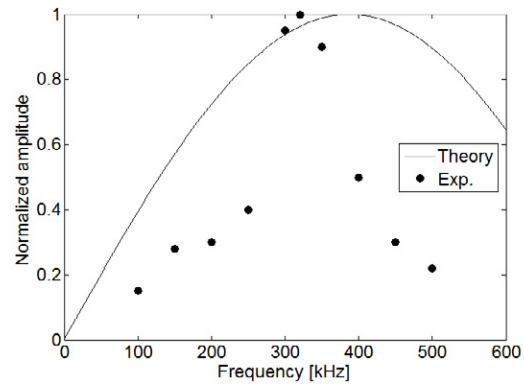


Fig. 5



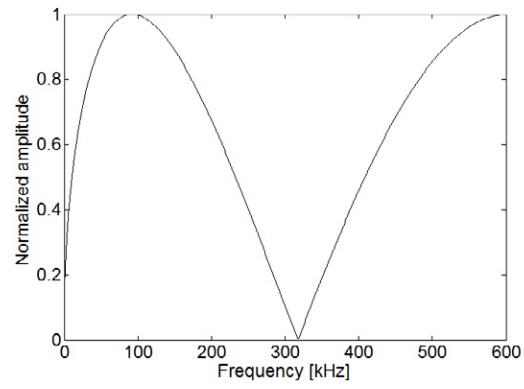
ACCEPTED MANUSCRIPT

Fig. 6



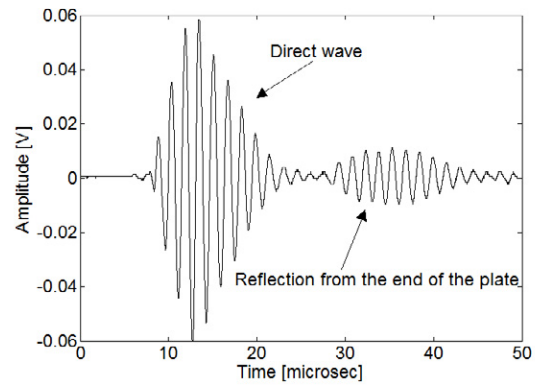
ACCEPTED MANUSCRIPT

Fig. 7



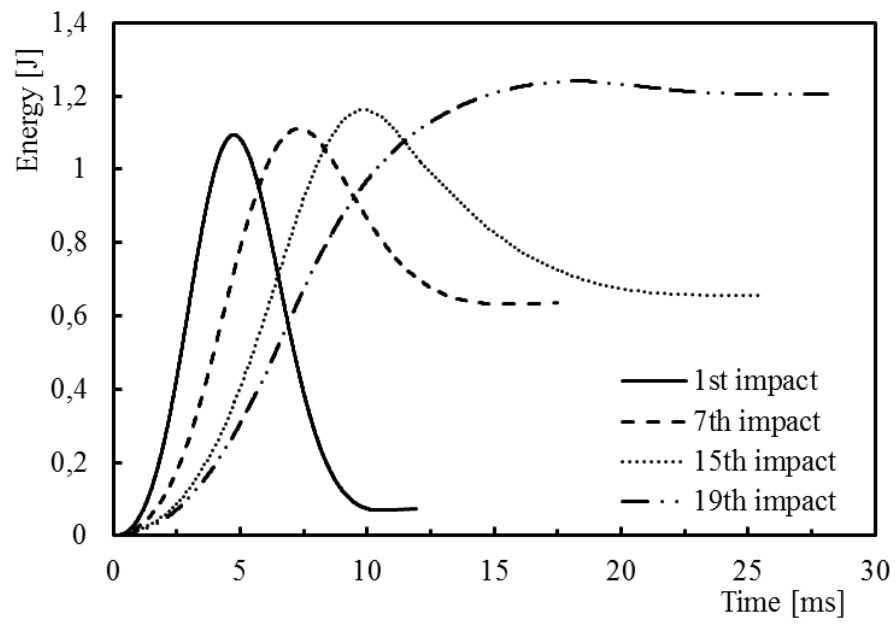
ACCEPTED MANUSCRIPT

Fig. 8



ACCEPTED MANUSCRIPT

Fig. 9



ACCEPTED MANUSCRIPT

ACCEPTED MANUSCRIPT

Fig. 10

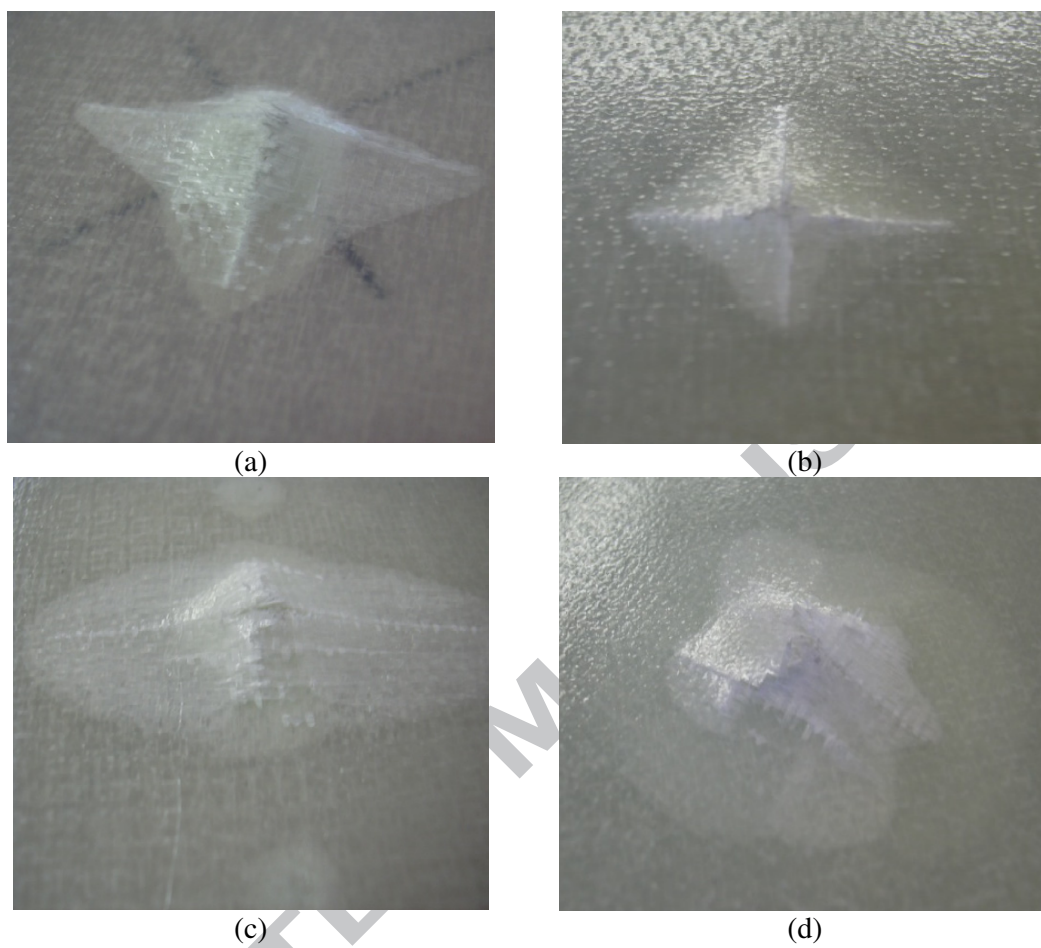
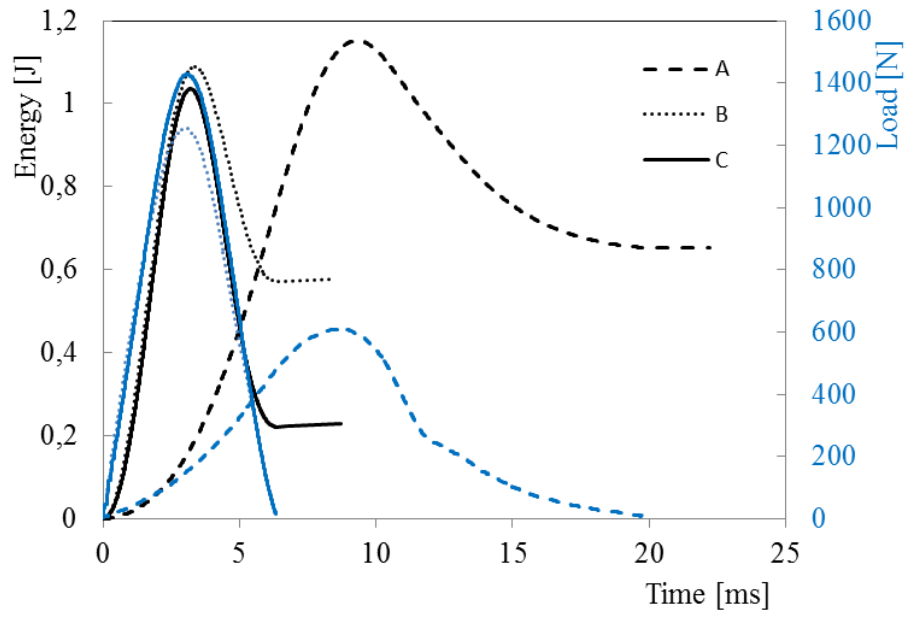
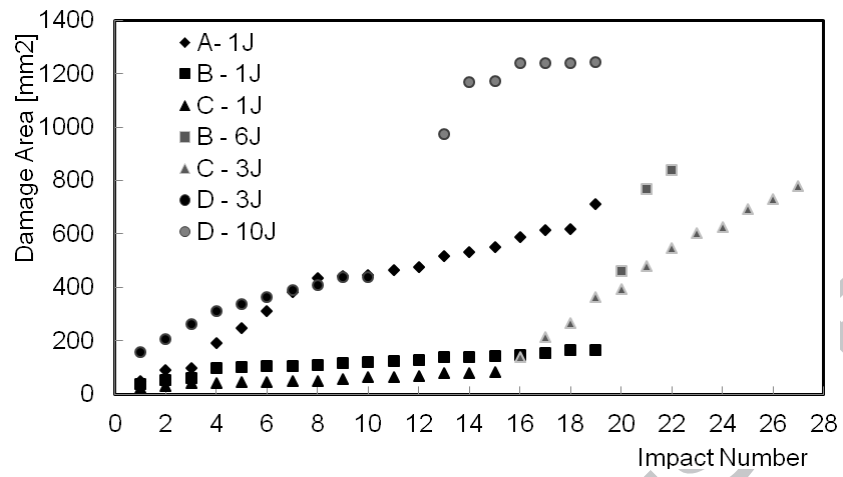


Fig. 11



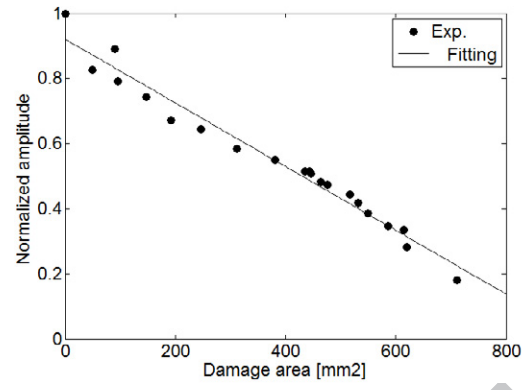
ACCEPTED MANUSCRIPT

Fig. 12



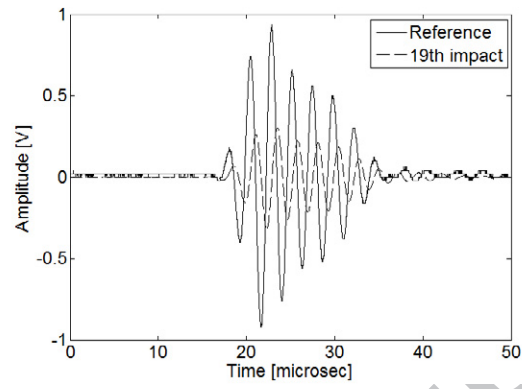
ACCEPTED MANUSCRIPT

Fig. 13



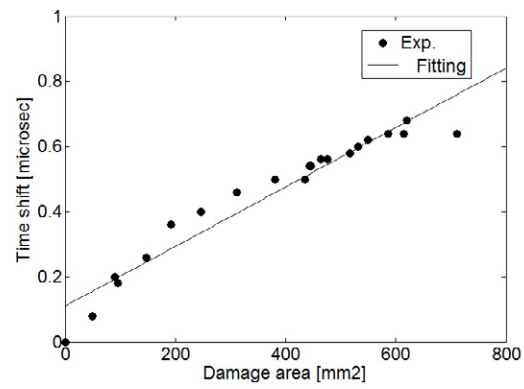
ACCEPTED MANUSCRIPT

Fig. 14



ACCEPTED MANUSCRIPT

Fig. 15



ACCEPTED MANUSCRIPT

Table caption

Table 1 - Composite laminated samples.

Table 2 - Mechanical properties from unidirectional glass/epoxy laminate.

Table 3 - Values of R^2 for all samples.

ACCEPTED MANUSCRIPT

Table 1

Samples	Stacking sequences	Thickness [mm]
A	$[0_2, 90_2]_s$	1
B	$[0_2, 90_2]_{2s}$	2.1
C	$[0, 90, 0, 90]_{2s}$	2.1
D	$[45_2, 90_2, -45_2, 0_2]_{2s}$	4.2

ACCEPTED MANUSCRIPT

Table 2

	E_1 [GPa]	$E_2=E_3$ [GPa]	$G_{12} = G_{13}$ [GPa]	G_{23} [GPa]	ν_2
	35.22	6.04	2.31	2.79	0.26
SD [%]	2.15	5.30	1.11	4.19	6.15

ACCEPTED MANUSCRIPT

Table 3

Samples	R^2	
	Amplitude	Time shift
A	0.968	0.936
B	0.182	0.790
C	0.895	0.988
D	0.190	0.992

ACCEPTED MANUSCRIPT